

Pair Production of Charged Higgs Bosons from Bottom-Quark Fusion

Hou Hong-Sheng², Ma Wen-Gan^{1,2}, Zhang Ren-You², Jiang Yi², Han Liang², Xing Li-Rong²

¹CCAST (World Laboratory), P.O.Box 8730, Beijing, 100080, People's Republic of China

²Department of Modern Physics, University of Science and Technology of China (USTC),
Hefei, Anhui 230026, People's Republic of China

Abstract

For very large values of $\tan\beta$, charged Higgs boson pair production at the Large Hadron Collider (LHC) from the scattering of two bottom quarks can proceed dominantly. We investigated the cross sections of charged Higgs boson pair production via the subprocess $b\bar{b} \rightarrow H^+H^-$ at the LHC including the next-to-leading order (NLO) QCD corrections in the minimal supersymmetric standard model (MSSM). We find that the SUSY QCD corrections to the relevant Yukawa coupling strength will significantly suppress or enhance the cross section depending on the sign of the higgsino mass parameter μ .

PACS: 14.80. Cp, 12.60.Jv, 12.38.Bx

I. Introduction

One of the most important missions of future high-energy experiments are to search for scalar Higgs bosons and explore the electroweak symmetry breaking mechanism. In the standard model (SM)[1], one doublet of complex scalar fields is needed to spontaneously break the symmetry, leading to a single neutral Higgs boson h^0 . But there exists the problem of the quadratically divergent contributions to the corrections to the Higgs boson mass. One of the good methods to solve this problem is to make supersymmetric (SUSY) extensions to the SM. Then the quadratic divergences of the Higgs mass can be cancelled by loop diagrams involving the supersymmetric partners of the SM particles exactly. The most attractive supersymmetric extension of the SM is the minimal supersymmetric standard model (MSSM) [2]. The MSSM requires the existence of two doublets of Higgs fields, to cancel anomalies and to give mass separately to up and down-type fermions. The MSSM predicts two CP-even neutral Higgs bosons h^0, H^0 , a pseudoscalar A^0 boson and a pair of charged scalar particles H^\pm . At the tree level, the MSSM Higgs sector has two free parameters: $\tan\beta = v_2/v_1$ the ratio of the vacuum expectation values of the two Higgs doublets and a Higgs boson mass, which we take to be m_{H^\pm} .

The discovery of the H^\pm would be a clear signal for the existence of physics beyond the Standard Model, with a strong hint towards supersymmetry. The CERN large hadron collider (LHC), which has the proton-proton colliding energy $\sqrt{s} = 14 \text{ TeV}$, will be a wonderful tool to look for new physics. At the LHC, light charged Higgs boson can be produced from the top quark decays $t \rightarrow b + H^+$ [3]. Heavy charged Higgs boson is mainly produced via the processes $g\bar{b} \rightarrow \bar{t}bH^+$ [4], $gg \rightarrow \bar{t}bH^+$ [5] and $qb \rightarrow q'bH^+$ [6]. Moreover, single charged Higgs boson production associated with a W boson, via tree-level $b\bar{b}$ annihilation and one-loop gg fusion, has been proposed and analyzed in Ref.[7].

At the LHC, charged Higgs boson also can be produced in pair production mode. There are three important H^+H^- production channels: (i) $q\bar{q} \rightarrow H^+H^-$, where $q = u, d, c, s, b$. (via Drell-Yan process, where a photon and a Z-boson are exchanged in the s -channel. In the case

of $q = b$, there are additional Feynman diagrams involving h^0 and H^0 in the s -channel and the top quark in the t -channel). For very large values of $\tan \beta$, due to the large contributions from the additional diagrams, the H^+H^- production proceeds dominantly via $b\bar{b}$ annihilation [8] [10]. (ii) $gg \rightarrow H^+H^-$ (via quarks and squarks loop) [9] [10]. (iii) $qq \rightarrow qqH^+H^-$ (via vector boson fusion) [11].

In the subprocess $b\bar{b} \rightarrow H^+H^-$, the initial state bottom quarks arise from gluon in the proton splitting into a collinear $b\bar{b}$ -pair, parameterized in terms of bottom quark distribution functions. In using a gluon density, the 'twin' process $gg \rightarrow b\bar{b}H^+H^-$ has been studied at LO in Ref.[12]. It is pointed out that the use of the b-quark density may overestimate the inclusive cross section due to crude approximations in the kinematics [13]. However, it is suggested that the bottom quark parton approximation maybe valid by choosing appropriate factorization scale [14]. Following the suggestion in Ref.[14], one looks at the transverse momentum distribution of the b-quarks in the process $gg \rightarrow b\bar{b}H^+H^-$, as shown in Fig.2 of Ref.[12], the most suitable factorization scale for $b\bar{b} \rightarrow H^+H^-$ is of order $m_{H^\pm}/5 \sim m_{H^\pm}/4$ which is much smaller than the usually used scale m_{H^\pm} .

In this paper, we study the specific process $pp \rightarrow b\bar{b} \rightarrow H^+H^- + X$ at the LHC with very large $\tan \beta$ in the MSSM. The NLO QCD corrections are calculated. The paper is organized as follow: In section II, we discuss the LO results of the subprocess $b\bar{b} \rightarrow H^+H^-$. In section III, we present the calculations of the NLO QCD corrections. In section 4, the numerical results, discussions and conclusions are presented.

II. The Leading Order Cross Section

The Feynman diagrams for the subprocess $b(p_1)\bar{b}(p_2) \rightarrow H^+(k_3)H^-(k_4)$ at the LO are shown in Fig.1, where $p_{1,2}$ and $k_{3,4}$ represent the four-momenta of the incoming partons and the outgoing particles, respectively.

We divide the tree-level amplitude into two parts and denote the expression as

$$M^0 = M_0^{(s)} + M_0^{(t)}, \quad (2.1)$$

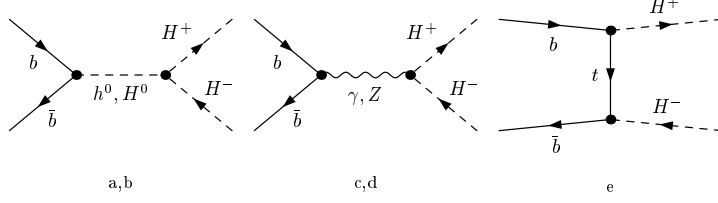


Figure 1: The tree level Feynman diagrams for $b\bar{b} \rightarrow H^+H^-$ subprocess.

where $M_0^{(s)}$ and $M_0^{(t)}$ represent the amplitudes arising from the s-channel diagram shown in Fig.1(a,b,c,d) and the t-channel diagram shown in Fig.1(e), respectively. The explicit expressions for the amplitudes $M_0^{(s)}$ and $M_0^{(t)}$ can be written as

$$\begin{aligned}
M_0^{(t)} &= i\bar{v}(p_2) \frac{(P_R g_{H^+tb}^{(1)} + P_L g_{H^+tb}^{(2)})(m_t + \not{p}_1 - \not{k}_3)(P_L g_{H^+tb}^{(1)} + P_R g_{H^+tb}^{(2)})}{\hat{t} - m_t^2} u(p_1), \\
M_0^{(s)} &= i\bar{v}(p_2) \left[\frac{g_{H^+H^-h^0} g_{h^0 b\bar{b}}}{\hat{s} - m_{h^0}^2} + \frac{g_{H^+H^-H^0} g_{H^0 b\bar{b}}}{\hat{s} - m_{H^0}^2} - \frac{Q_b e^2 (\not{k}_3 - \not{k}_4)}{\hat{s}} \right. \\
&\quad \left. - \frac{(c_w^2 - s_w^2) e^2 (\not{k}_3 - \not{k}_4) (s_w^2/3 - P_L/2)}{2c_w^2 s_w^2 (\hat{s} - m_Z^2)} \right] u(p_1), \tag{2.2}
\end{aligned}$$

where $\hat{s} = (p_1 + p_2)^2$, $\hat{t} = (p_1 - k_3)^2$ and $\hat{u} = (p_1 - k_4)^2$ are the usual Mandelstam variables.

$P_{L,R} = (1 \mp \gamma_5)/2$, $s_w = \sin \theta_w$, $c_w = \cos \theta_w$, $Q_b = -1/3$. The couplings are defined below,

$$\begin{aligned}
g_{H^+tb}^{(1)} &= \frac{iem_t}{\sqrt{2}m_W s_w \tan \beta}, & g_{H^+tb}^{(2)} &= \frac{ie\bar{m}_b(\mu_r) \tan \beta}{\sqrt{2}m_W s_w}, \\
g_{h^0 b\bar{b}} &= \frac{ie\bar{m}_b(\mu_r) \sin \alpha}{2m_W s_w \cos \beta}, & g_{H^0 b\bar{b}} &= -\frac{ie\bar{m}_b(\mu_r) \cos \alpha}{2m_W s_w \cos \beta}, \\
g_{H^+H^-h^0} &= -\frac{iem_W}{s_w} (\sin(\beta - \alpha) + \frac{\cos(2\beta) \sin(\alpha + \beta)}{2c_w^2}), \\
g_{H^+H^-H^0} &= -\frac{iem_W}{s_w} (\cos(\beta - \alpha) - \frac{\cos(2\beta) \cos(\alpha + \beta)}{2c_w^2}), \tag{2.3}
\end{aligned}$$

where α is the mixing angle which leads to the physical Higgs eigenstates h^0 and H^0 . $\bar{m}_b(\mu_r)$ is $\overline{\text{MS}}$ running mass of the bottom quark. We neglected the bottom quark mass during our calculation except in the Yukawa couplings.

Then the LO cross section for the subprocess $b\bar{b} \rightarrow H^+H^-$ is obtained by using the following formula:

$$\hat{\sigma}^0(\hat{s}, b\bar{b} \rightarrow H^+H^-) = \frac{1}{16\pi\hat{s}^2} \int_{\hat{t}_{min}}^{\hat{t}_{max}} d\hat{t} \sum |M^0|^2, \tag{2.4}$$

where $\hat{t}_{max,min} = (m_{H^\pm} - \frac{1}{2}\hat{s}) \pm \frac{1}{2}\sqrt{\hat{s}^2 - 4m_{H^\pm}^2\hat{s}}$. The summation is taken over the spins and colors of initial and final states, and the bar over the summation denotes averaging over the spins and colors of initial partons.

III. NLO QCD Corrections in the MSSM

The NLO QCD corrections to $pp \rightarrow b\bar{b} \rightarrow H^+H^- + X$ in the MSSM can be separated into two parts: the virtual corrections arising from loop diagrams and the real corrections.

3.1 Virtual Corrections

The virtual corrections in the MSSM to subprocess $b\bar{b} \rightarrow H^+H^-$ consist of self-energy, vertex and box diagrams which are depicted in Figs.2-3. Fig.2 shows the diagrams of the SM-like QCD corrections from quark and gluon loops, and Fig.3 presents the diagrams of the so called 'pure' SUSY QCD corrections from squark and gluino loops. There exist both ultraviolet(UV) and soft/collinear infrared(IR) singularities in the amplitudes for the SM-like diagrams in Fig.2. The amplitudes for SUSY QCD diagrams(Fig.3) only contain UV singularities. In our calculation, we adopt the 't Hooft-Feynman gauge and all the divergences are regularized by using dimensional regularization method in $d = 4 - 2\epsilon$ dimensions.

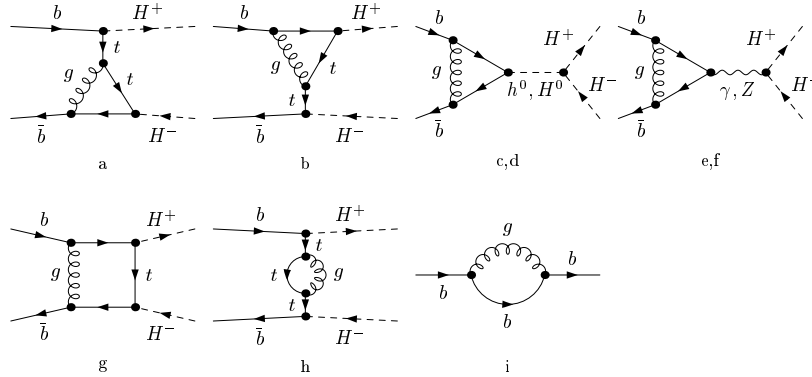


Figure 2: The one-loop SM-like QCD correction Feynman diagrams for $b\bar{b} \rightarrow H^+H^-$ subprocess.

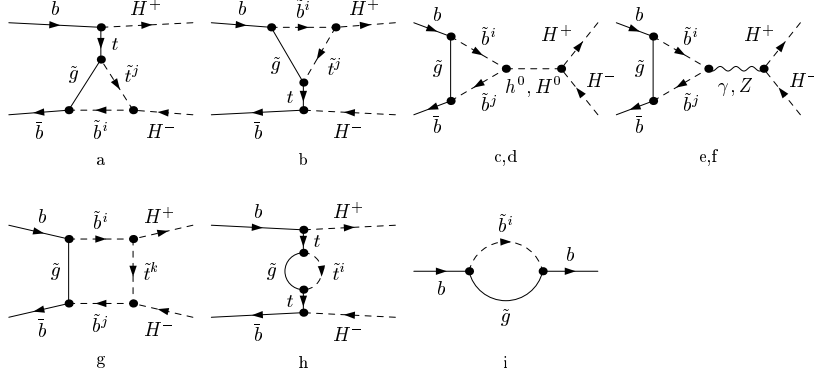


Figure 3: The one-loop 'pure' SUSY QCD correction Feynman diagrams for $b\bar{b} \rightarrow H^+H^-$ subprocess.

In order to remove the UV divergences, we need to renormalize the wave functions of the external fields and the Yukawa couplings $h^0 - b - \bar{b}$, $H^0 - b - \bar{b}$, $H^- - t - \bar{b}$. We renormalize the top quark mass in the on-mass-shell (OS) scheme. For the renormalization of the bottom quark mass in the Yukawa couplings, we employ the modified Minimal Subtraction ($\overline{\text{MS}}$) scheme. The relevant renormalization constants in this work can be expressed as

$$\begin{aligned}
\frac{\delta m_t}{m_t} &= \left(\frac{\delta m_t}{m_t}\right)^{(QCD)} + \left(\frac{\delta m_t}{m_t}\right)^{(SQCD)} \\
&= -\frac{\alpha_s}{4\pi} C_F \{ (4B_0 + 2B_1)(m_t^2, m_t^2, 0) - 1 \} \\
&\quad - \frac{\alpha_s}{4\pi} C_F \left\{ \sum_{i=1}^2 \left[B_1 - \frac{m_{\tilde{g}}}{m_t} \sin(2\theta_t(-1)^i B_0) \right] (m_t^2, m_{\tilde{g}}^2, m_{t_i}^2) \right\}, \\
\delta Z_b^L &= (\delta Z_b^L)^{(QCD)} + (\delta Z_b^L)^{(SQCD)} \\
&= -\frac{\alpha_s}{4\pi} C_F B_0(0, 0, 0) + \frac{\alpha_s}{2\pi} C_F \left[B_1(0, m_{\tilde{g}}^2, m_{b_1}^2) \cos^2 \theta_{\tilde{b}} + B_1(0, m_{\tilde{g}}^2, m_{b_2}^2) \sin^2 \theta_{\tilde{b}} \right], \\
\delta Z_b^R &= (\delta Z_b^R)^{(QCD)} + (\delta Z_b^R)^{(SQCD)} \\
&= -\frac{\alpha_s}{4\pi} C_F B_0(0, 0, 0) + \frac{\alpha_s}{2\pi} C_F \left[B_1(0, m_{\tilde{g}}^2, m_{b_1}^2) \sin^2 \theta_{\tilde{b}} + B_1(0, m_{\tilde{g}}^2, m_{b_2}^2) \cos^2 \theta_{\tilde{b}} \right], \\
\frac{\delta m_b}{m_b} &= \left(\frac{\delta m_b}{m_b}\right)^{(QCD)} + \left(\frac{\delta m_b}{m_b}\right)^{(SQCD)} \\
&= -\frac{\alpha_s}{4\pi} 3C_F \Delta + \frac{\alpha_s}{4\pi} C_F \Delta,
\end{aligned} \tag{3.1}$$

with $\Delta = \frac{1}{\epsilon} - \gamma_E + \ln(4\pi)$ and $C_F = \frac{4}{3}$. We have divided the above renormalization constants into two parts, The terms in Eqs.(3.1) with upper indexes 'QCD' means the SM-like QCD parts, and those with 'SQCD' represent the 'pure' SUSY QCD parts. The SM-like QCD part arises from the loop of quark and gluon, the 'pure' SUSY QCD part comes from the loop of squark and gluino.

The virtual corrections to the cross section of subprocess $b\bar{b} \rightarrow H^+H^-$ can be written as

$$\hat{\sigma}^V(\hat{s}, b\bar{b} \rightarrow H^+H^-) = \frac{1}{16\pi\hat{s}^2} \int_{\hat{t}_{min}}^{\hat{t}_{max}} d\hat{t} \, 2Re \sum \overline{[(M^V)^\dagger M^0]}, \quad (3.2)$$

with $\hat{t}_{max,min}$ and the summation with bar mean the same operations as those declared in Eq.(2.4). M^V is the renormalized amplitude for virtual corrections. After renormalization procedure, $\hat{\sigma}^V$ is UV-finite. Nevertheless, it still contains the soft/collinear IR singularities

$$d\hat{\sigma}^V|_{IR} = \left[\frac{\alpha_s}{2\pi} \frac{\Gamma(1-\epsilon)}{\Gamma(1-2\epsilon)} \left(\frac{4\pi\mu_r^2}{\hat{s}} \right)^\epsilon \right] d\hat{\sigma}^0 \left(\frac{A_2^V}{\epsilon^2} + \frac{A_1^V}{\epsilon} \right), \quad (3.3)$$

where

$$A_2^V = -2C_F, \quad A_1^V = -3C_F. \quad (3.4)$$

The soft divergences will be cancelled by adding the real gluon emission corrections, and the remaining collinear divergences can be absorbed into the parton distribution functions, which will be discussed in the following subsections.

3.2 Real Gluon Emission Corrections $b\bar{b} \rightarrow H^+H^- + g$

The $O(\alpha_s)$ corrections to $b\bar{b} \rightarrow H^+H^-$ due to real gluon emission (shown in Fig.4) give the origin of IR singularities which cancel exactly the analogous singularities present in the $O(\alpha_s)$ virtual corrections mentioned in above subsection. These singularities can be either of soft or collinear nature and can be conveniently isolated by slicing the $b\bar{b} \rightarrow H^+H^- + g$ phase space into different regions defined by suitable cutoffs, a method which goes under the general name of phase space slicing (PPS)[15].

In this work, we calculate the cross section for the $2 \rightarrow 3$ process

$$b(p_1) + \bar{b}(p_2) \rightarrow H^+(k_3) + H^-(k_4) + g(k_5) \quad (3.5)$$

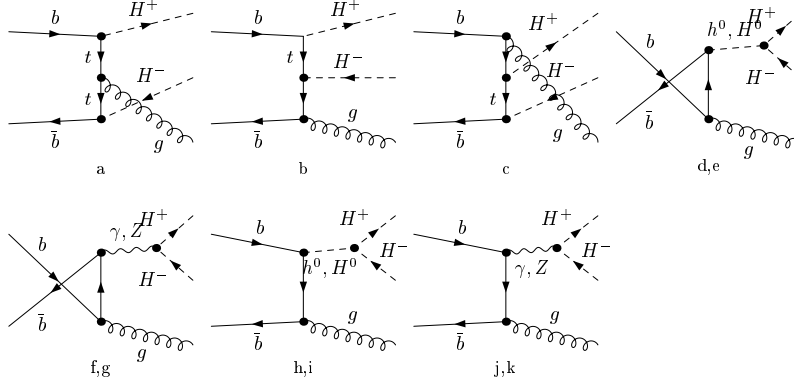


Figure 4: Feynman diagrams for $b\bar{b} \rightarrow H^+H^- + g$ subprocess at the lowest level.

by using the two cutoff phase space slicing method. We define the invariants

$$\begin{aligned}\hat{s} &= (p_1 + p_2)^2, \quad \hat{t} = (p_1 - k_3)^2, \quad \hat{u} = (p_1 - k_4)^2, \\ \hat{t}_{15} &= (p_1 - k_5)^2, \quad \hat{t}_{25} = (p_2 - k_5)^2\end{aligned}\tag{3.6}$$

and describe this method briefly as follows. Firstly, by introducing an arbitrary small soft cutoff δ_s we separate the $2 \rightarrow 3$ phase space into two regions, according to whether the energy of the emitted gluon is soft, i.e. $E_5 \leq \delta_s \sqrt{\hat{s}}/2$, or hard, i.e. $E_5 > \delta_s \sqrt{\hat{s}}/2$. The partonic real cross section can be written as

$$\hat{\sigma}_g^R(b\bar{b} \rightarrow H^+H^-g) = \hat{\sigma}_g^S(b\bar{b} \rightarrow H^+H^-g) + \hat{\sigma}_g^H(b\bar{b} \rightarrow H^+H^-g),\tag{3.7}$$

where $\hat{\sigma}_g^S$ is obtained by integrating over the soft region of the emitted gluon phase space. $\hat{\sigma}_g^S$ contains all the soft IR singularities. Secondly, to isolate the remaining collinear singularities from $\hat{\sigma}_g^H$, we further decompose $\hat{\sigma}_g^H$ into a sum of hard-collinear (HC) and hard-non-collinear ($\overline{\text{HC}}$) terms by introducing another cutoff δ_c named collinear cutoff

$$\hat{\sigma}_g^H(b\bar{b} \rightarrow H^+H^-g) = \hat{\sigma}_g^{\text{HC}}(b\bar{b} \rightarrow H^+H^-g) + \hat{\sigma}_g^{\overline{\text{HC}}}(b\bar{b} \rightarrow H^+H^-g).\tag{3.8}$$

The HC regions of the phase space are those where any invariant t_{15}, t_{25} becomes smaller in magnitude than $\delta_c \hat{s}$, while at the same time the emitted gluon remains hard. $\hat{\sigma}_g^{\text{HC}}$ contains the

collinear divergences. In the soft and HC region, $\hat{\sigma}_g^S$ and $\hat{\sigma}_g^{\text{HC}}$ can be obtained by performing the phase space integration in d -dimension analytically. In the $\overline{\text{HC}}$ region, $\hat{\sigma}_g^{\overline{\text{HC}}}$ is finite and can be evaluated in four dimensions using standard Monte Carlo techniques[16]. The cross sections, $\hat{\sigma}_g^S$, $\hat{\sigma}_g^{\text{HC}}$ and $\hat{\sigma}_g^{\overline{\text{HC}}}$, depend on the two arbitrary parameters, δ_s and δ_c . However, in the total real gluon emission hadronic cross section σ_g^R , after mass factorization, the dependence on these arbitrary cutoffs cancels, as will be explicitly shown in Sec. 4. This constitutes an important check of our calculation.

The differential cross section in the soft region is given as

$$d\hat{\sigma}_g^S = d\hat{\sigma}^0 \left[\frac{\alpha_s}{2\pi} \frac{\Gamma(1-\epsilon)}{\Gamma(1-2\epsilon)} \left(\frac{4\pi\mu_r^2}{\hat{s}} \right)^\epsilon \right] \left(\frac{A_2^S}{\epsilon^2} + \frac{A_1^S}{\epsilon} + A_0^S \right), \quad (3.9)$$

with

$$A_2^S = 2C_F, \quad A_1^S = -4C_F \ln \delta_s, \quad A_0^S = 4C_F \ln^2 \delta_s. \quad (3.10)$$

The differential cross section $d\sigma_g^{\text{HC}}$ for $pp \rightarrow b\bar{b} \rightarrow H^+H^- + X$ can be written as

$$\begin{aligned} d\sigma_g^{\text{HC}} &= d\hat{\sigma}^0 \left[\frac{\alpha_s}{2\pi} \frac{\Gamma(1-\epsilon)}{\Gamma(1-2\epsilon)} \left(\frac{4\pi\mu_r^2}{\hat{s}} \right)^\epsilon \right] \left(-\frac{1}{\epsilon} \right) \delta_c^{-\epsilon} [2P_{bb}(z, \epsilon) G_{b/P}(x_1/z) G_{\bar{b}/P}(x_2) \\ &+ (x_1 \leftrightarrow x_2)] \frac{dz}{z} \left(\frac{1-z}{z} \right)^{-\epsilon} dx_1 dx_2. \end{aligned} \quad (3.11)$$

where $G_{b,\bar{b}/P}(x)$ is the bare parton distribution function of $b(\bar{b})$ quark in proton. $P_{bb}(z, \epsilon)$ is the d -dimensional unregulated ($z < 1$) splitting function related to the usual Altarelli-Parisi splitting kernel [17]. $P_{bb}(z, \epsilon)$ can be written explicitly as

$$\begin{aligned} P_{bb}(z, \epsilon) &= P_{bb}(z) + \epsilon P'_b(z), \\ P_{bb}(z) &= C_F \frac{1+z^2}{1-z}, \quad P'_b(z) = -C_F(1-z). \end{aligned} \quad (3.12)$$

3.3 Real Corrections $gb(\bar{b}) \rightarrow H^+H^- + b(\bar{b})$

In addition to the real gluon emission $b\bar{b} \rightarrow H^+H^- + g$, there are also processes $gb(\bar{b}) \rightarrow H^+H^- + b(\bar{b})$ at this order of perturbation theory, as shown in Fig.5.

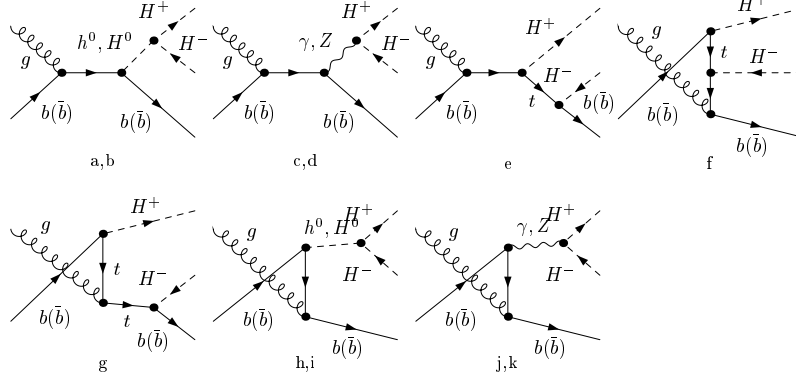


Figure 5: Feynman diagrams for $gb(\bar{b}) \rightarrow H^+H^- + b(\bar{b})$.

The contributions from these processes only contain the initial state collinear singularities. Using the method described above, we split the phase space into two regions: collinear region and non-collinear region.

$$\hat{\sigma}_b^R[gb(\bar{b}) \rightarrow H^+H^- + b(\bar{b})] = \hat{\sigma}_b^C[gb(\bar{b}) \rightarrow H^+H^- + b(\bar{b})] + \hat{\sigma}_b^{\overline{C}}[gb(\bar{b}) \rightarrow H^+H^- + b(\bar{b})] \quad (3.13)$$

Also $\hat{\sigma}_b^{\overline{C}}$ is finite and can be evaluated in four dimensions using standard Monte Carlo techniques. The differential cross section of $pp \rightarrow gb(\bar{b}) \rightarrow H^+H^- + b(\bar{b})$ $d\sigma_b^C$ can be written as

$$\begin{aligned} d\sigma_b^C &= d\hat{\sigma}^0 \left[\frac{\alpha_s}{2\pi} \frac{\Gamma(1-\epsilon)}{\Gamma(1-2\epsilon)} \left(\frac{4\pi\mu_r^2}{\hat{s}} \right)^\epsilon \right] \left(-\frac{1}{\epsilon} \right) \delta_c^{-\epsilon} [2P_{bg}(z, \epsilon) G_{g/P}(x_1/z) G_{b/P}(x_2) \\ &+ (x_1 \leftrightarrow x_2)] \frac{dz}{z} \left(\frac{1-z}{z} \right)^{-\epsilon} dx_1 dx_2. \end{aligned} \quad (3.14)$$

with

$$\begin{aligned} P_{bg}(z, \epsilon) &= P_{bg}(z) + \epsilon P'_{bg}(z), \\ P_{bg}(z) &= \frac{1}{2}[z^2 + (1-z)^2], \quad P'_{bg}(z) = -z(1-z). \end{aligned} \quad (3.15)$$

3.4 NLO QCD Cross Section for $pp \rightarrow b\bar{b} \rightarrow H^+H^- + X$

After adding the renormalized virtual corrections and the real corrections, the hadronic cross sections still contain the collinear divergences, which can be absorbed into the redefini-

tion of the distributions functions at NLO. Using the $\overline{\text{MS}}$ scheme, the scale dependent NLO parton distribution functions are given as [15]

$$G_{i/P}(x, \mu_f) = G_{i/P}(x) + \sum_j \left(-\frac{1}{\epsilon}\right) \left[\frac{\alpha_s}{2\pi} \frac{\Gamma(1-\epsilon)}{\Gamma(1-2\epsilon)} \left(\frac{4\pi\mu_r^2}{\mu_f^2} \right)^\epsilon \right] \int_z^1 \frac{dz}{z} P_{ij}(z) G_{j/P}(x/z). \quad (3.16)$$

By using above definition, we get a NLO QCD parton distribution function counter-terms which are combined with the hard collinear contributions to result in the $O(\alpha_s)$ expression for the remaining collinear contributions:

$$\begin{aligned} d\sigma^{coll} &= d\hat{\sigma}^0 \left[\frac{\alpha_s}{2\pi} \frac{\Gamma(1-\epsilon)}{\Gamma(1-2\epsilon)} \left(\frac{4\pi\mu_r^2}{\hat{s}} \right)^\epsilon \right] \{ 2\tilde{G}_{b/P}(x_1, \mu_f) G_{\bar{b}/P}(x_2, \mu_f) \\ &+ 2 \left[\frac{A_1^{sc}(b \rightarrow bg)}{\epsilon} + A_0^{sc}(b \rightarrow bg) \right] G_{b/P}(x_1, \mu_f) G_{\bar{b}/P}(x_2, \mu_f) \\ &+ (x_1 \leftrightarrow x_2) \} dx_1 dx_2, \end{aligned} \quad (3.17)$$

where

$$A_1^{sc}(b \rightarrow bg) = C_F(2\ln \delta_s + 3/2), \quad A_0^{sc} = A_1^{sc} \ln\left(\frac{\hat{s}}{\mu_f^2}\right), \quad (3.18)$$

and

$$\tilde{G}_{b/P}(x, \mu_f) = \sum_{j=b,g} \int_x^{1-\delta_s\delta_{bj}} \frac{dy}{y} G_{j/P}(x/y, \mu_f) \tilde{P}_{bj}(y), \quad (3.19)$$

with

$$\tilde{P}_{ij}(y) = P_{ij} \ln\left(\delta_c \frac{1-y}{y} \frac{\hat{s}}{\mu_f^2}\right) - P'_{ij}(y). \quad (3.20)$$

We can observe that the sum of the soft (Eq.(3.9)), collinear(Eq.(3.17)), and ultraviolet renormalized virtual correction (Eq.(3.3)) terms is finite, i.e.,

$$\begin{aligned} A_2^S + A_2^V &= 0, \\ A_1^S + A_1^V + 2A_1^{sc}(b \rightarrow bg) &= 0. \end{aligned} \quad (3.21)$$

The final result for the total $O(\alpha_s)$ correction consists of two parts of contributions: a two-body term $\sigma^{(2)}$ and a three-body term $\sigma^{(3)}$.

$$\begin{aligned} \sigma^{(2)} &= \frac{\alpha_s}{2\pi} \int dx_1 dx_2 d\hat{\sigma}^0 \{ G_{b/P}(x_1, \mu_f) G_{\bar{b}/P}(x_2, \mu_f) [A_0^S + A_0^V + 2A_0^{sc}(b \rightarrow bg)] \\ &+ 2\tilde{G}_{b/P}(x_1, \mu_f) G_{b/P}(x_2, \mu_f) + (x_1 \leftrightarrow x_2) \}. \end{aligned} \quad (3.22)$$

And

$$\sigma^{(3)} = \int dx_1 dx_2 [G_{b/P}(x_1, \mu_f) G_{\bar{b}/P}(x_2, \mu_f) + (x_1 \leftrightarrow x_2)] d\hat{\sigma}^{(3)}, \quad (3.23)$$

with

$$d\hat{\sigma}^{(3)} = \frac{1}{2\hat{s}_{12}} \left\{ \int_{\overline{\text{HC}}} \sum |M_3(b\bar{b} \rightarrow H^+ H^- g)|^2 d\Gamma_3 + 2 \int_{\overline{\text{C}}} \sum |M_3(gb \rightarrow H^+ H^- b)|^2 d\Gamma_3 \right\}. \quad (3.24)$$

Finally, the NLO total cross section for $pp \rightarrow b\bar{b} \rightarrow H^+ H^- + X$ is

$$\sigma^{NLO} = \sigma^0 + \sigma^{(2)} + \sigma^{(3)}. \quad (3.25)$$

IV. Numerical Results and Discussion

In this section, we present the numerical results of the cross section for the charged Higgs boson pair production from bottom quark fusion at the LHC. In the numerical evaluation, we take the SM parameters as: $m_t = 178.1$ GeV, $m_Z = 91.1876$ GeV, $m_W = 80.425$ GeV and $\alpha_{EW}(m_W) = 1/128$. We use the two-loop formula for the running strong coupling α_s with $\alpha_s(m_Z) = 0.1187$ [18]. We adopt the CTEQ6L1 parton distribution function for the LO cross sections and CTEQ6M for NLO results [19]. The factorization scale is taken as $\mu_f = m_{H^\pm}/4$ and the renormalization scale is taken as $\mu_r = m_{H^\pm}$ by default unless otherwise stated. We present the results involving the SM-like QCD and the total SUSY QCD corrections in following two subsections separately.

4.1 The SM-like QCD Corrections

In this subsection, we present the cross sections including only the SM-like QCD corrections. That means we consider only the SM-like QCD diagrams showed in Figure 2 and let the renormalization constants only being related to their SM-like QCD parts in Eq.(3.1) when we calculate the virtual corrections. The $\overline{\text{MS}}$ bottom quark mass $\overline{m}_b(\mu_r)$ can be evaluated

by using the one-loop renormalization group improved formula with the bottom quark pole mass taken to be $m_b = 4.7$ GeV.

$$(\overline{m}_b(\mu_r))^{QCD} = m_b \left(1 - \frac{4}{3} \frac{\alpha_s(m_b)}{\pi}\right) \left[\frac{\alpha_s(\mu_r)}{\alpha_s(m_b)}\right]^{(c_0/b_0)}, \quad b_0 = \frac{1}{4\pi} \left(\frac{11}{3}N - \frac{2}{3}n_f\right), \quad c_0 = \frac{1}{\pi}. \quad (4.1)$$

with $N = 3$ is the number of colors and $n_f = 5$ is the number of active flavors.

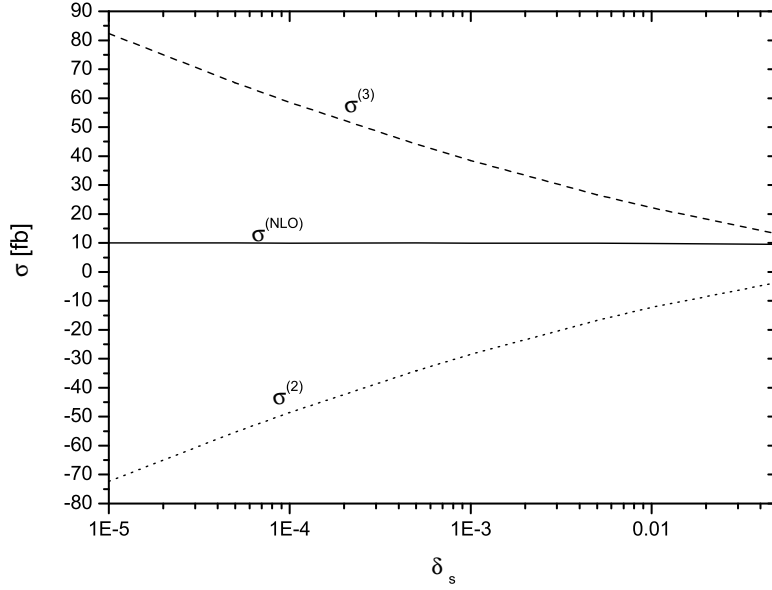


Figure 6: The cross sections of $pp \rightarrow b\bar{b} \rightarrow H^+H^- + X$ as the functions of the cutoff δ_s at the LHC.

Fig.6 shows that our NLO-QCD result of the cross section of does not depend on the arbitrary cutoffs δ_s and δ_c introduced by using the two cutoff phase space slicing method at the LHC. The two-body($\sigma^{(2)}$) and three-body($\sigma^{(3)}$) contributions and the NLO cross section (σ^{NLO}) are shown as a function of the soft cutoff δ_s with the collinear cutoff $\delta_c = \delta_s/50$. $\tan \beta = 40$, $m_{H^\pm} = 180$ GeV and $\mu_f = \mu_r = m_{H^\pm}$. We can see the NLO cross section σ^{NLO} is independent of the cutoffs. In the following numerical calculations, we take $\delta_s = 10^{-4}$ and $\delta_c = \delta_s/50$.

In Fig.7, we show the dependence of the total cross sections for $pp \rightarrow b\bar{b} \rightarrow H^+H^- + X$ on the renormalization scale and the factorization scale with $\tan \beta = 40$, $m_{H^\pm} = 180$ GeV. In the left plot of Fig.7, the renormalization scale is taken to be $\mu_r = m_{H^\pm}$ while the factorization

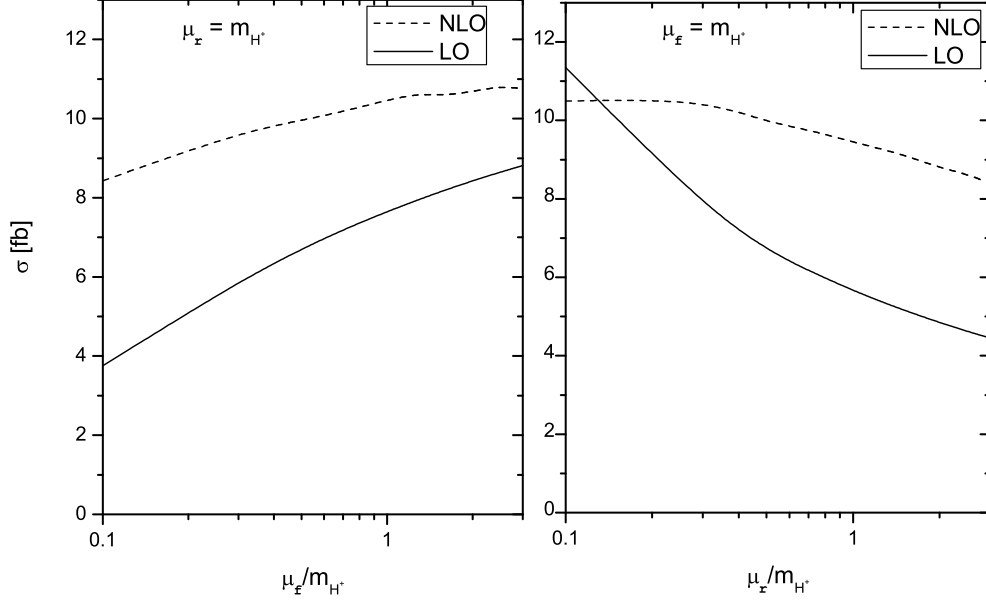


Figure 7: The cross sections of $pp \rightarrow b\bar{b} \rightarrow H^+H^- + X$ as the functions of renormalization scale μ_r and factorization scale μ_f at the LHC.

scale varies in the region $0.1m_{H^\pm} \sim 3m_{H^\pm}$. In the right plot of Fig.7, we take $\mu_f = m_{H^\pm}$ and $0.1m_{H^\pm} < \mu_r < 3m_{H^\pm}$. A significant reduction of the scale dependence can be observed for the NLO cross sections, thus the reliability of the NLO QCD predictions has been improved substantially.

Fig.8 shows the dependence of the LO and NLO cross sections for $pp \rightarrow b\bar{b} \rightarrow H^+H^- + X$ on the charged Higgs mass m_{H^\pm} . $\tan\beta$ is taken to be 40 (upper lines) and 20 (lower lines). m_{H^\pm} varies from 180 GeV to 500 GeV. The total cross section can reach 10 fb for small values of m_{H^\pm} with very large $\tan\beta$. In Fig.9, the dependence of the $pp \rightarrow b\bar{b} \rightarrow H^+H^- + X$ cross section on $\tan\beta$ are studied for $m_{H^\pm} = 180$ GeV and 400 GeV. The cross sections increase rapidly with the increasing of $\tan\beta$ from 10 to 50.

4.2 The Results Including the Total SUSY QCD Corrections

The relevant SUSY parameters in our calculation are: the parameters $M_{\tilde{Q},\tilde{U},\tilde{D}}$ and $A_{t,b}$ in squark mass matrices, the higgsino mass parameter μ and the masses of the gluino $m_{\tilde{g}}$. The

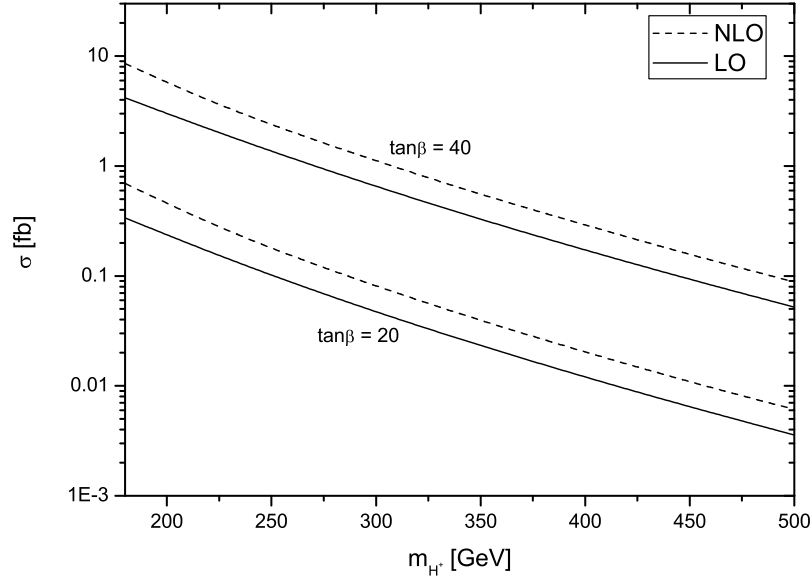


Figure 8: The cross sections for $pp \rightarrow b\bar{b} \rightarrow H^+H^- + X$ as the functions of m_{H^\pm} at the LHC.

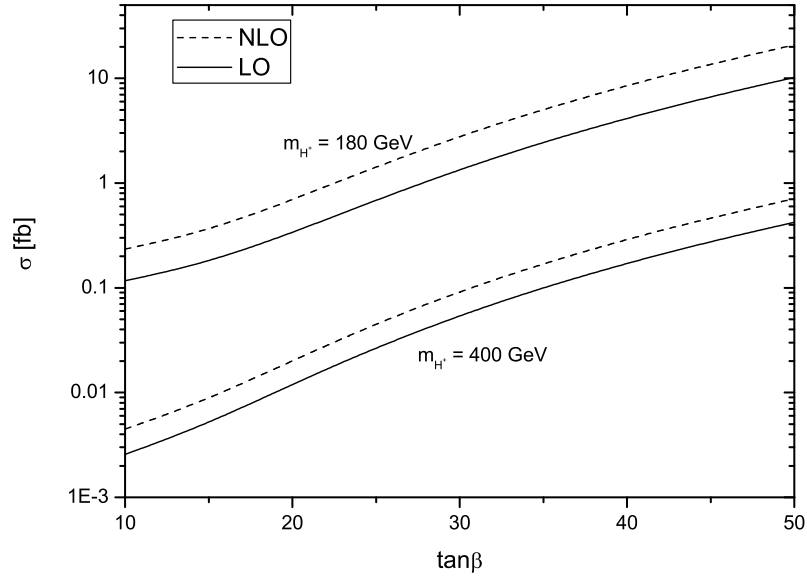


Figure 9: The cross sections for $pp \rightarrow b\bar{b} \rightarrow H^+H^- + X$ as the functions of $\tan \beta$ at the LHC.

squark mass matrix is defined as

$$\mathcal{M}_{\tilde{q}}^2 = \begin{pmatrix} m_{\tilde{q}_L}^2 & a_q m_q \\ a_q m_q & m_{\tilde{q}_R}^2 \end{pmatrix} \quad (4.2)$$

with

$$\begin{aligned} m_{\tilde{q}_L}^2 &= M_{\tilde{Q}}^2 + m_q^2 + m_Z^2 \cos 2\beta (I_3^q - e_q \sin^2 \theta_W), \\ m_{\tilde{q}_R}^2 &= M_{\{\tilde{U}, \tilde{D}\}}^2 + m_q^2 + m_Z^2 \cos 2\beta e_q \sin^2 \theta_W \\ a_q &= A_q - \mu \{\cot \beta, \tan \beta\}, \end{aligned} \quad (4.3)$$

for {up, down} type squarks. I_3^q and e_q are the third component of the weak isospin and the electric charge of the quark q . The chiral states \tilde{q}_L and \tilde{q}_R are transformed into the mass eigenstates \tilde{q}_1 and \tilde{q}_2 :

$$\begin{pmatrix} \tilde{q}_1 \\ \tilde{q}_2 \end{pmatrix} = R^{\tilde{q}} \begin{pmatrix} \tilde{q}_L \\ \tilde{q}_R \end{pmatrix}, \quad R^{\tilde{q}} = \begin{pmatrix} \cos \theta_{\tilde{q}} & \sin \theta_{\tilde{q}} \\ -\sin \theta_{\tilde{q}} & \cos \theta_{\tilde{q}} \end{pmatrix}. \quad (4.4)$$

Then the mass eigenvalues $m_{\tilde{q}_1}$ and $m_{\tilde{q}_2}$ are given by

$$\begin{pmatrix} m_{\tilde{q}_1}^2 & 0 \\ 0 & m_{\tilde{q}_2}^2 \end{pmatrix} = R^{\tilde{q}} \mathcal{M}_{\tilde{q}}^2 (R^{\tilde{q}})^\dagger \quad (4.5)$$

For simplicity, we assume $M_{\tilde{Q}} = M_{\tilde{U}} = M_{\tilde{D}} = A_t = A_b = m_{\tilde{g}} = 500$ GeV, $\mu = 200$ GeV.

In the MSSM, for large $\tan \beta$ the counter term to m_b can be very large due to the 'pure' SUSY QCD (gluino-mediated) graph. Here we absorb the gluino contributions into the tree-level Yukawa couplings [20]. In such a way we obtain the $\overline{\text{MS}}$ bottom quark mass \overline{m}_b including the total SUSY QCD contributions,

$$(\overline{m}_b(\mu_r))^{SQCD} = (\overline{m}_b(\mu_r))^{QCD} - \frac{\alpha_s}{4\pi} C_F m_b \left\{ \sum_{i=1}^2 [B_1^{fin} - \frac{m_{\tilde{g}}}{m_b} \sin(2\theta_{\tilde{b}}) (-1)^i B_0^{fin}] (m_b^2, m_{\tilde{g}}^2, m_{\tilde{b}_i}^2) \right\} \quad (4.6)$$

where the notations B_1^{fin} and B_0^{fin} mean the operations of taking the finite parts of the two-point integral functions. As shown in a series papers, the SUSY QCD contributions to the bottom quark running mass can be written as [21]

$$(\overline{m}_b(\mu_r))^{SQCD} \simeq \frac{(\overline{m}_b(\mu_r))^{QCD}}{1 + \Delta m_b}, \quad (4.7)$$

where

$$\Delta m_b = \frac{2\alpha_s}{3\pi} \mu m_{\tilde{g}} \tan \beta I(m_{\tilde{b}_1}, m_{\tilde{b}_2}, m_{\tilde{g}}), \quad (4.8)$$

with

$$I(a, b, c) = \frac{1}{(a^2 - b^2)(b^2 - c^2)(a^2 - c^2)} (a^2 b^2 \log \frac{a^2}{b^2} + b^2 c^2 \log \frac{b^2}{c^2} + c^2 a^2 \log \frac{c^2}{a^2}). \quad (4.9)$$

Indeed, if all supersymmetry breaking mass parameters and μ are of equal size, one get an interesting limit of Eq.(4.8), depending on the sign of μ [22]

$$\Delta m_b = \text{sign}(\mu) \frac{\alpha_s(Q = M_{SUSY})}{3\pi} \tan \beta. \quad (4.10)$$

Hence, Δm_b does not decouple in the limit of large values of the supersymmetry breaking masses and the sign of μ is the decisive factor in determining whether the SUSY QCD corrections will enhance or suppress the LO cross section of $pp \rightarrow b\bar{b} \rightarrow H^+ H^- + X$ process.

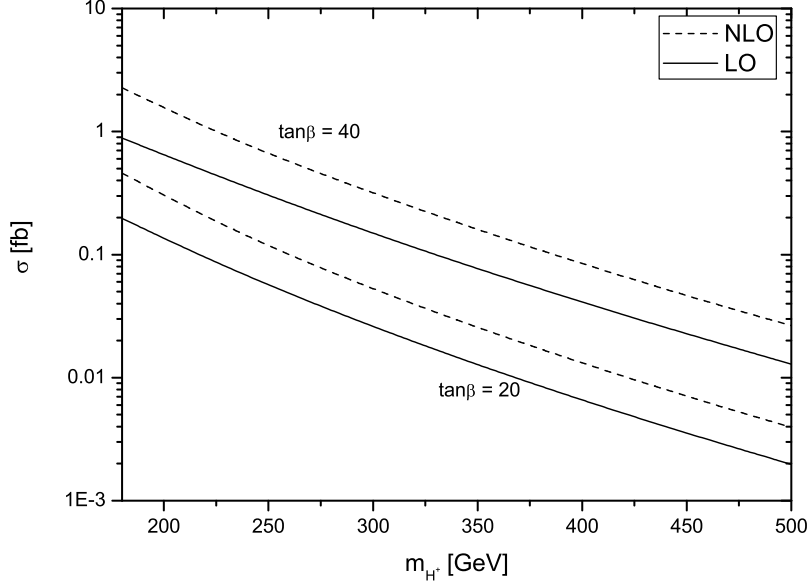


Figure 10: The cross sections of $pp \rightarrow b\bar{b} \rightarrow H^+ H^- + X$ including the total SUSY QCD corrections as the functions of m_{H^\pm} at the LHC.

In our calculations we use Eq. (4.6) to calculate the $\overline{\text{MS}}$ running bottom quark mass. In Fig.10, we show the dependence of the LO and NLO cross sections of $pp \rightarrow b\bar{b} \rightarrow H^+ H^- + X$

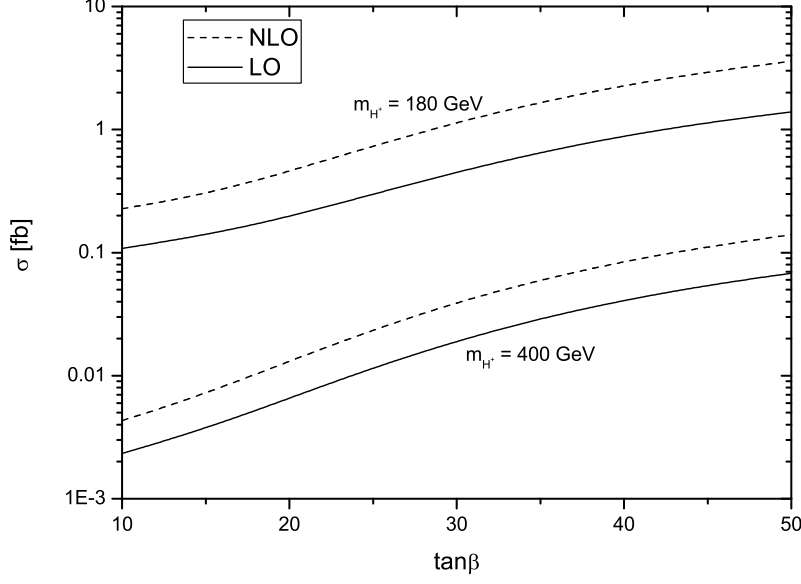


Figure 11: The cross sections of $pp \rightarrow b\bar{b} \rightarrow H^+H^- + X$ including the total SUSY QCD corrections as the functions of $\tan\beta$ at the LHC.

process including the total SUSY QCD corrections on the charged Higgs mass m_{H^\pm} . From Fig.8 and Fig.10, we can see that the curves in Fig.10 are much lower than the corresponding ones in Fig.8, because after including the total SUSY QCD contributions, $(\overline{m}_b(\mu_r))^{SQCD}$ is much smaller than $(\overline{m}_b(\mu_r))^{QCD}$, in case that the sign of μ is positive and $\tan\beta$ is large (see Eq. (4.10)). In Fig.11, the dependence of the cross sections including the total SUSY QCD contributions on $\tan\beta$ are shown. It shows that both the LO and NLO SUSY QCD corrected cross sections increase with the increment of the value of $\tan\beta$.

In summary, we have computed the production of charged Higgs boson pair via the bottom quark fusion subprocess in the MSSM at the LHC. With very large $\tan\beta$ values, the $b\bar{b} \rightarrow H^+H^-$ subprocess can become the dominant one in the charged Higgs boson pair production at the LHC. We also investigate its LO cross section and the NLO SUSY QCD correction to the $pp \rightarrow b\bar{b} \rightarrow H^+H^- + X$ process. We find that the NLO SUSY QCD corrections are significant for the charged Higgs boson pair production at the LHC. Our numerical results show also that after including the total SUSY QCD contributions with large $\tan\beta$, the \overline{MS}

bottom quark mass \overline{m}_b will receive large corrections, and it will significantly suppress or enhance the cross section depending on the sign of the higgsino mass parameter μ .

Acknowledgments: This work was supported in part by the National Natural Science Foundation of China and special fund sponsored by China Academy of Science.

References

- [1] S. Weinberg, Phys. Rev. Lett. **19**, 1264 (1967); S. Glashow, Nucl. Phys. B **22**, 579 (1961); A. Salam, in *Elementary Particle Theory*, edited by N. Svartholm, p367 (1968).
- [2] H. P. Nilles Phys. Rep. **110**, 1 (1984); H. E. Haber and G. L. Kane, Phys. Rep. **117**, 75 (1985); J. F. Gunion, H. E. Haber, Nucl. Phys. B **272**, 1 (1986).
- [3] Z. Kunszt and F. Zwirner, Nucl.Phys. B **385**, 3 (1992).
- [4] J. F. Gunion, H. E. Haber, F. E. Paige, W.-K. Tung and S. S. D. Willenbrock, Nucl. Phys. B **294**, 621 (1987); R. M . Barnett, H. E. Haber and D. E. Soper Nucl. Phys. B **306**, 697 (1988); F. I. Olness and W.-K. Tung, Nucl. Phys. B **308**, 813 (1988); V. Barger, R. J. N. Philips and D. P. Roy, Phys. Lett. B **324**, 236 (1994).
- [5] J. L. Diaz-Cruz and O. A. Sampayo, Phys. Rev. D **50**, 6820 (1994).
- [6] S. Moretti and K. Odagiri, Phys. Rev. D **55**, 5627 (1997).
- [7] D. A. Dicus, J. L. Hewett, C. Kao and T. G. Rizzo, Phys. Rev. D **40**, 787 (1989); S. Moretti and K. Odagiri, Phys. Rev. D **59**, 055008 (1999); A. A. Barrientos Bendez and B. A. Kniehl, Phys. Rev. D **59**, 015009 (1999); A. A. Barrientos Bendez and B. A. Kniehl, Phys. Rev. D **61**, 097701 (2000); A. A. Barrientos Bendez and B. A. Kniehl, Phys. Rev. D **63**, 015009 (2001); O. Brein, W. Hollik, and S. Kanemura, Phys. Rev. D **63**, 095001 (2001).
- [8] E. Eichten, I. Hinchliffe, K. Lane and C. Quigg, Rev. Mod. Phys. **56**, 579 (1984).

- [9] S.S.D. Willenbrock, Phys. Rev. D **35**, 173 (1987); Y. Jiang, W.-G. Ma, L. Han, M. Han and Z.-H. Yu, J. Phys. G **23**, 385 (1997), Erratum, *ibidem* G **23**, 1151 (1997); A. Krause, T. Plehn, M. Spira and P.M. Zerwas, Nucl. Phys. B **519**, 85 (1998); A. Belyaev, M. Drees, O.J.P. Eboli, J.K. Mizukoshi and S.F. Novaes, Phys. Rev. **D60**, 075008 (1999); A. Belyaev, M. Drees and J.K. Mizukoshi, Eur. Phys. J. C **17**, 337 (2000); O. Brein and W. Hollik, Eur. Phys. J. C **13**, 175 (2000).
- [10] A.A. Barrientos Bendezú and B.A. Kniehl, Nucl. Phys. B **568**, 305 (2000);
- [11] S. Moretti, J. Phys. G **28**, 2567 (2002).
- [12] S. Moretti and J. Rathsman, Eur. Phys. J. C **33**, 41 (2004).
- [13] D. Rainwater, M. Spira and D. Zeppenfeld, MAD-PH-02-1260, hep-ph/0203187; M. Spira, PSI-PR-02-19, hep-ph/0211145.
- [14] T. Plehn, Phys. Rev. D **67**, 014018 (2003); F. Maltoni, Z. Sullivan and W. Willenbrock, Phys. Rev. D **67**, 093005 (2003); E. Boos and T. Plehn, Phys.Rev. D **69**, 094005 (2004); R. V. Harlander and W. B. Kilgore, Phys.Rev. D **68**, 013001 (2003).
- [15] B.W. Harris and J.F. Owens, Phys. Rev. D **65** 094032(2002)
- [16] G.P. Lepage, J. Comput. Phys. **27**,192(1978)
- [17] G. Altarelli and G. Parisi, Nucl. Phys. B**126** 298 (1977).
- [18] S. Eidelman, *et al.*, Phys. Lett. **B529**, (2004)1.
- [19] J. Pumplin *et al.*, JHEP 0207, 012 (2002); D. Stump *et al.*, JHEP 0310, 046 (2003).
- [20] C. Weber, H. Eberl, W. Majerotto, Phys.Rev. D **68**, 093011(2003).
- [21] L. Hall, R. Rattazzi and U. Sarid, Phys. Rev. D**50**, 7048 (1994); M. Carena, M. Olechowski, S. Pokorski and C. E. Wagner, Nucl. Phys. B **426**, 269 (1994); D. Pierce, J. Bagger, K. Matchev and R. Zhang, Nucl. Phys. B **491**, 3(1997).

[22] M. Carena, D. Garcia, U. Nierste and C.E. Wagner, Nucl. Phys. B **577**, 88 (2000).